Short communication

Green immobilized Ag NPs over magnetic Fe$_3$O$_4$ NPs using *Pomegranate* juice induces apoptosis via P53 and signal transducer and activator of transcription 3 signaling pathways in human gastric cancer cells

Meng Meng [a], Dongyun Xue [b],*

[a] *Department of Gastrointestinal Surgery, Shandong Provincial Third Hospital, Shandong University, Jinan 250031, China*
[b] *Department of gastroenterology, Shandong Provincial Third Hospital, Shandong University, Jinan, 250031, China*

ABSTRACT

Herein, we demonstrate the bio-inspired synthesis Ag NPs over surface of magnetic Fe$_3$O$_4$ NPs by using *Pomegranate* juice (PJ). The *Pomegranate* juice was used as an eco-friendly media which acted as green reductant and the in-situ stabilizer for the synthesized Ag NPs. The inherent structural and morphological properties of the as-synthesized Fe$_3$O$_4$@PJ/Ag NPs was analyzed by electron microscopy (SEM and TEM), energy dispersive X-ray spectroscopy (EDX), elemental mapping, vibrating sample magnetometer (VSM), X-ray diffraction (XRD) and inductively coupled plasma-optical emission spectroscopy (ICP-OES). The anti-gastric cancer properties of the biogenic Fe$_3$O$_4$@PJ/Ag NPs were assessed against gastric cancer cell lines. The Fe$_3$O$_4$@PJ/Ag material could significantly combat the growth of GC1415, NCI-N87 and MKN45 cancer cells in a time and concentration-dependent manner, as determined by MTT assay. Fe$_3$O$_4$@PJ/Ag NPs induces cell apoptosis, accompanied by the up regulation of pro-apoptotic markers (Bax and cleaved caspase-8) and down regulation of the anti-apoptotic marker, Bcl-2. Moreover, Fe$_3$O$_4$@PJ/Ag NPs inhibits colony formation compared to their matched control. More significantly, the molecular pathway analysis of Fe$_3$O$_4$@PJ/Ag NPs-treated cells revealed that Fe$_3$O$_4$@PJ/Ag NPs enhances p53 expression, while inhibiting the expression of total and phosphorylated Signal Transducer and Activator of Transcription 3 (STAT3) in cell lines, suggesting p53 and STAT3 are the main key players behind the biological events provoked by the extract in human gastric cancer cells. The antioxidant activity of Fe$_3$O$_4$@PJ/Ag NPs was also determined by DPPH method. The significantly good IC$_{50}$ value indicated the material as an excellent antioxidant.

1. Introduction

Apoptosis is considered as a vital process in cancer where the cancer cells have the characteristics to strive to escape from apoptosis and continue to proliferate. Therefore, the ability to induce apoptosis in these cells is a major goal in the ailment of cancer. The process of apoptosis, or programmed cell death, is a conserved, genetically controlled method that is crucial in regulating growth rate, cell proliferation, development, and body health [1–3]. Current findings have shown that the reactive oxygen species production in target cells is one of the regulators of the apoptotic process. During normal cellular activity, reactive oxygen species produce oxygen and nitrogen. At low physiological levels, these reactive oxygen species act as messengers of redox and intracellular regulation. While at high levels, they cause oxidative changes, inhibiting protein function and promoting cell death [2–4]. To prevent redox imbalance and oxidative damage, there are defense barriers that include antioxidant enzymes such as thioredoxin reductase, catalase, glutathione peroxidase and superoxide dismutase, and non-enzymatic antioxidants including ascorbic acid, vitamin E and glutathione [4,5]. The effects of oxidative nanoparticles have been revealed to be greater in cancer cells that proliferate faster than normal cells. The previous studies introduced the increase in ROS production as the primary mechanism of toxicity in the cancer cell lines. Oxidized nanoparticles have also been shown to inhibit cell proliferation and induce apoptosis significantly in cancer cells. Thus, oxidized nanoparticles have anti-proliferative ability in cancer cells. However, its toxicity to normal cells is a challenge that must be addressed [5–7].

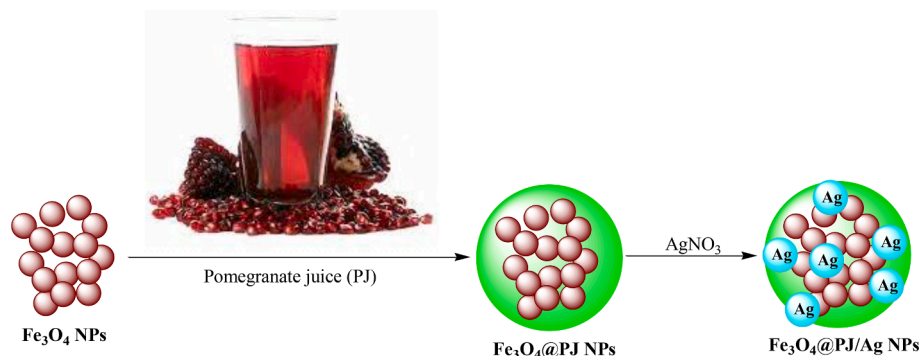Nanotechnology is one of the new and convenient branches of

---

Scheme 1. The biogenic synthesis of magnetic Fe$_3$O$_4$@PJ/Ag NPs mediated by *Pomegranate* juice.

material science that has been utterly granted by researchers for the progress and development of medical sciences [7–11]. In addition to medical sciences, this technology has also been largely adopted in military, agricultural, diagnostic methods, magnetic imaging, sensors and rapid material detection [12–14]. Researchers use this technology to diagnose and treat many diseases. Nanotechnology, as its name implies, deals with nanoscale objects. Different nanomaterials have been processed that are used in surgery, dentistry, various experiments in experimental sciences, biomechanical systems, fight against microorganisms, etc. Although many studies have been done on the effect of nanoparticles, scientists still do not have complete control over the range of its effects. In the discussion of imaging methods, less invasive methods are much more appropriate, so nanoparticles are ideal candidates for developing such imaging methods [13–16]. Nanotechnology uses engineered materials to produce physiological responses and nerve stimulation while minimizing side effects. Unlike conventional systems such as tablets and solutions, nanoparticles intelligently control and perpetuate the distribution of drugs in different parts and make them more effective [17–20]. Metallic nanoparticles such as silver nanoparticles have been used for the treatment of several cancers such as prostate, bladder, lung, gastric and colorectal cancers [21–25]. Many experiments have indicated that the medicinal plants increase the anticancer effects of the silver nanoparticles when they are used for green-synthesizing of the nanoparticles [26–32].

In recent times, it has been an incessant effort paid by the researchers in the advancement of physicochemical, catalytic and biological properties of advanced functionalized nanomaterials. In this particular study, we report the biogenic synthesis of Ag NPs immobilized on magnetite NPs using *Pomegranate* juice as a media for eco-benevolent reduction of metal ions as well as efficient stabilization of the NPs from agglomeration, aerial oxidation, corrosion etc (Scheme 1). The as-synthesized Fe$_3$O$_4$@PJ/Ag NPs exhibited excellent potential in the resistance of gastric cancer.

2. Experimental

2.1. Synthesis of magnetic Fe$_3$O$_4$@PJ/Ag NPs

Fe$_3$O$_4$ NPs were synthesized following well reported method by co-precipitating the hydroxides of Fe^{2+} (FeSO$_4$·7H$_2$O, 4.2 g) and Fe^{3+} (FeCl$_3$·6H$_2$O, 6.1 g) into DI water (100 mL) using ammoniac media. The brown Fe$_3$O$_4$ NPs were retrieved by magnetic decantation, washed with DI H$_2$O to neutral and dried in air at 80 °C. In the subsequent steps, 0.5 g Fe$_3$O$_4$ NPs were suspended by sonication in DI H$_2$O (100 mL) for 20 min followed by the addition of *Pomegranate* juice (20 mL). The mixture was then stirred at room temperature for 12 h to afford the Fe$_3$O$_4$@PJ nanocomposite particle. It was isolated magnetically, washed several times with DI water and again dispersed by sonication in 100 mL water. The precursor of Ag, a solution of AgNO$_3$ (25 mg in 20 mL H$_2$O) was then introduced into the dispersion and the mixture was swirled at room

temperature for 5 h. The Fe$_3$O$_4$@PJ/Ag nanocomposite was finally isolated magnetically and rinsed with H$_2$O to vent the unwanted adhered substances (Scheme 1). The desired nanocomposite was dried in vacuum at 40 °C and the Ag content was determined by ICP-AES method to be 0.13 mmol/g.

2.2. DPPH assay protocol

The Fe$_3$O$_4$@PJ/Ag nanocomposite solutions were prepared in varied dilutions (1 to 1000 µg/mL) from phenolic powder. A reference solution of BHT, a synthetic antioxidant, was also prepared in methanol. An equal volume of purple colored DPPH methanol solution was mixed to the sample solution (2 mL each) and the mixture was stirred vigorously. After 30 min, absorbance of the faded pale yellow solution of the mixture was measured at UV–vis spectrophotometer at a wavelength of 517 nm [33–35]. The % inhibition capacity was calculated based on the following formula, where A stands for the corresponding absorbance.

$$\text{Inhibition}\,(\%) = \frac{\text{Sample A.}}{\text{Control A.}}\,x100$$

2.3. anti-Gastric cancer assay protocol

The method is derived from the activity of succinate dehydrogenase enzyme of cell mitochondria, which converts the yellow MTT solution to insoluble crystals of purple formazan which can be measured with an ELISA reader after dissolving in DMSO dimethyl sulfoxide. 10^4 cells were transferred to a 96-well plate and incubated at 37 °C for 24 h. Then various concentrations of the nanocomposite were treated with them and incubated under the same conditions for 24 and 48 h. This was followed by the addition of 10 µl of MTT solution (5 mg/ml) to each well and incubated again for 3 h. Then 100 µl of DMSO was replaced with MTT incubated and left in the dark for half an hour. DMSO dissolves the produced formazan crystals to form a purple-colored solution, which indicates the bioavailability of the treated cells. The plate's optical absorption was finally measured at 570 nm [36a].

$$\text{Cell viability}\,(\%) = \frac{\text{Sample A.}}{\text{Control A.}}\,x100$$

To analyze the cell cycle, 10^6 cells were put in 200 mm Petri dishes for 36 h. Synchronized cells (G0 phase) were treated with Fe$_3$O$_4$@PJ/Ag NPs for 54 h. Then, the DNA was then stained by the FXCycle PI/RNase staining solution at 60 mg/ml. Cells in the G2/M, S and G0/G1 phases were quantified by the Flow Jo software. Cellular apoptosis was assessed by the ApoScreenAnnex in V-fluorescein isothiocyanate (FITC)/7-amino-actinomycin D (7-AAD) Apoptosis Kit as per the manufacturer's protocol [36b].

Soft agar colony formation assay was performed for determining the cells ability to grow in an anchorage-independent manner. In immunoblotting analysis, 10^6 cells were put in Petri dishes and treated with the Fe$_3$O$_4$@PJ/Ag NPs material for 54 h. Protein lysates equal amounts
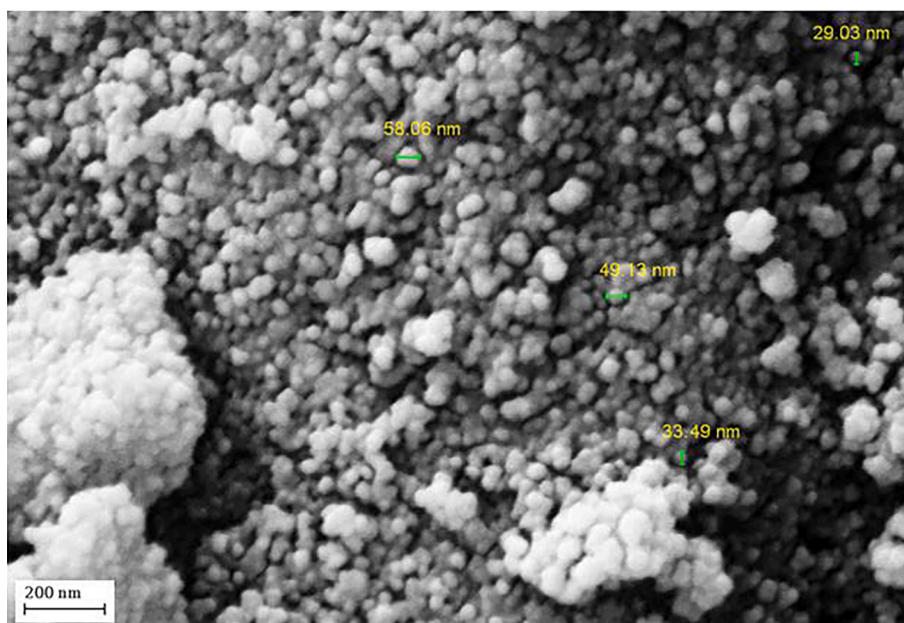
Fig. 1. SEM image of $Fe_3O_4@PJ/Ag$ NPs.

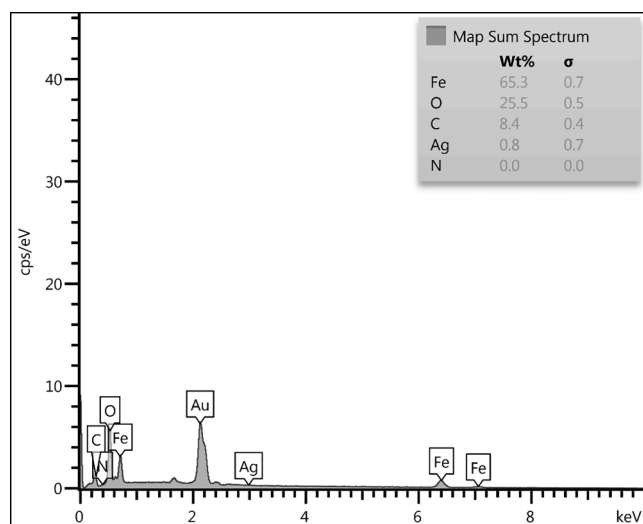**Fig. 2.** EDX spectrum of $Fe_3O_4@PJ/Ag$ NPs.

were run on 10 % polyacrylamide gels and transferred onto PVDF membranes. The membranes were incubated with the following primary antibodies overnight; rabbit anti-phosphorylated-STAT3, mouse anti-STAT3, rabbit anti-p53,mouse anti-cleaved caspase-8,mouse anti-Bcl-2and mouse anti-Bax. PVDF membranes were re-probed with rabbit anti-GAPDH to prove the proteins equal loading. Quantification was done by the Image J software and the bands' intensities was normalized to GAPDH to assess the relative protein expression [36b].

3. Results and discussion

Herein, we have developed a bio-inspired method for immobilizing Ag NPs over *Pomegranate* juice phytochemicals functionalized magnetic Fe_3O_4 NPs. The plant biomolecules also facilitated the green reduction of the metal ions as well as in situ stabilization of the nanomaterial. In the stepwise post-functionalization pathway the Fe_3O_4 MNPs were initially modified with the phyto-biomolecues and then Ag^+ ions gets adsorbed over the $Fe_3O_4@PJ$ composite. The electron rich organo-functions
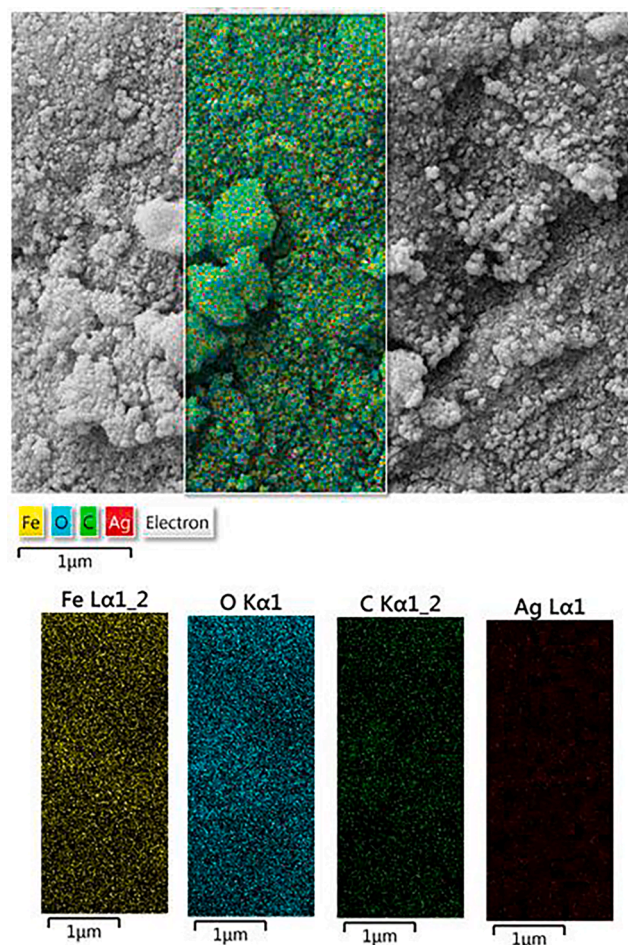

Fig. 3. Elemental mapping of $Fe_3O_4@PJ/Ag$ NPs.

subsequently carry out the in *situ* green reduction of the ions and stabilization of the NPs (Scheme 1). The as-synthesized material was then characterized by different advanced instrumental methods like SEM,
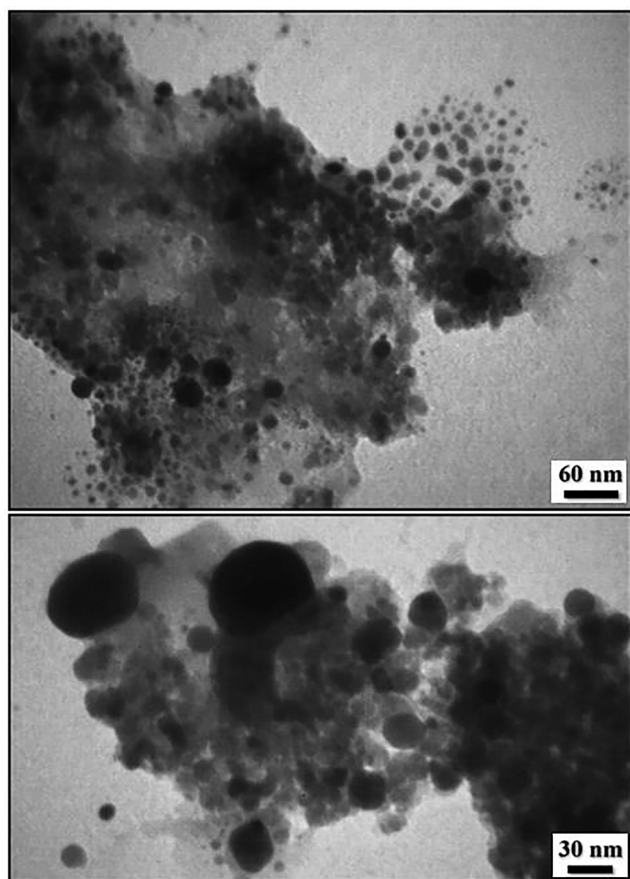
Fig. 4. TEM images of Fe_3O_4@PJ/Ag NPs.

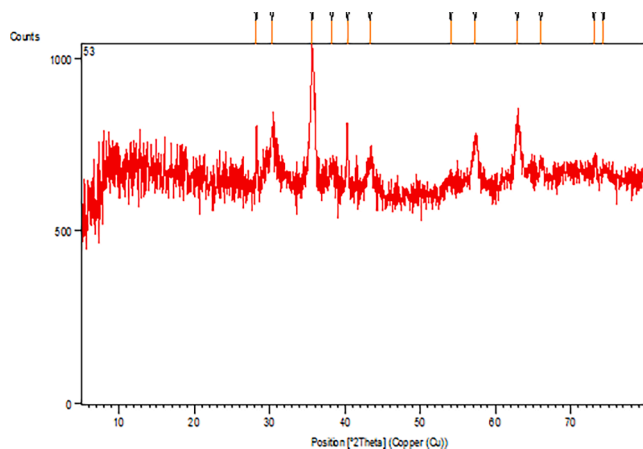**Fig. 5.** XRD pattern of Fe_3O_4@PJ/Ag NPs.

EDX, TEM, ICP-OES, VSM and XRD.

The morphological features, particle size and textures of Fe_3O_4@PJ/Ag NPs were ascertained by TEM and SEM study (Fig. 1,4). Fig. 1 clearly describes the particles are of quasi-spherical in shape. From SEM image however the distinction between Ag and Fe_3O_4 NPs cannot be possible. There are two different colored particles, white and grey and looks like a homogeneous blend between the two kinds. The material looks agglomerated, obviously due to manual sample preparation.

Chemical composition of the Fe_3O_4@PJ/Ag NPs was determined from EDX analysis, equipped with SEM instrument. As can be seen from Fig. 2, the profile contains Fe and Ag as metallic constitution and C, N and O as non-metals. The latter ones are indicative of plant biomolecular
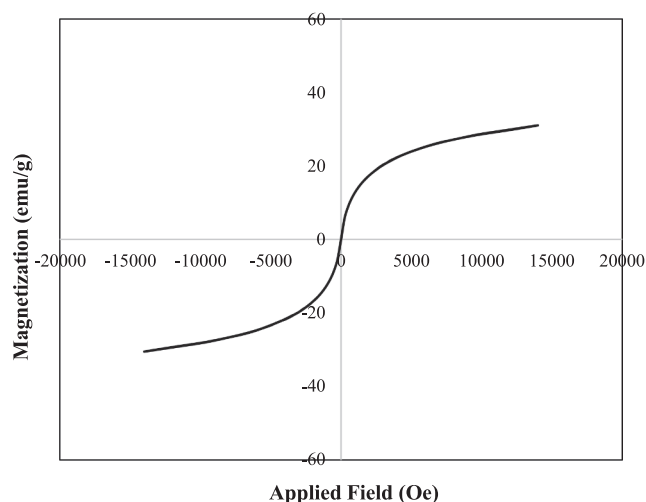

Fig. 6. VSM analysis of Fe_3O_4@PJ/Ag NPs.

association. The Au peak appears due to the gold vapor deposition over the sample prior to analysis. Constitution wise, Fe weighs the major (65.3 %) and Ag as a very minor quantity (0.8 %). The EDX analysis data were further detailed using elemental mapping study. Fig. 3 demonstrates the output of X-ray scanning of a segment of SEM image. Evidently, the elemental map shows very uniform distribution of the Fe, C, O and Ag atomic species throughout the material surface.

TEM analysis was carried out in order of intricate and intrinsic studies of the material surface. As Fig. 4 depicts, the particles are spherically shaped. A thin and continuous layer of the *Pomegranate* phytomolecules can be noticed around the material surface. The two different kinds of particles are obvious from their colors, grey and black, representing the Fe_3O_4 and Ag NPs. Ag NPs (10–20 nm) seem to be larger than the Fe_3O_4 NPs (20–30 nm).

XRD analysis was performed in order to validate the material crystallinity, its phases and purity. Fig. 5 exhibits the corresponding profile having a single phase, justifying a united molecular entity of the assembled constitutions. The material seems to be highly crystalline, showing six significant Bragg signals of Fe_3O_4 NPs at 2θ = 30.1, 35.5, 43.5, 54.1, 56.8, 63.1°, attributed to diffraction on (2 2 0), (3 1 1), (4 0 0), (4 2 2), (5 1 1) and (4 4 0) crystal planes respectively, being confirmed with standard (JCPDS file no. 65–3107). The extra peaks appeared at 2θ = 39.1°, 44.4°, 64.5° and 77.4° are allocated to the (1 1 1), (2 0 0), (2 2 0) and (3 1 1) crystal planes of Ag *fcc*.

Being an iron based magnetic material, VSM analysis seems ubiquitous for the Fe_3O_4@PJ/Ag NPs, in order to study its magnetic properties. On exposure to a band of external magnetic field of −20kOe to + 20kOe, the output results a magnetic hysteresis curve having the saturation magnetization (*M*s) value of 31.4 emu/g (Fig. 6). The nature validates it to be a superparamagnetic material. The *M*s value is quite low from the unmodified bare ferrite NPs, obviously due to surface modification with non-magnetic plant biomolecules and the Ag NPs.

Many researches in the field of biology and medicine are dedicated to radicals such as reactive oxygen species (ROS). In many living organisms, it is required for normal cell metabolic processes such as phagocytosis, reduction of inflammation, cell division and collagen synthesis [27,29]. Nevertheless, there is now considerable evidence that ROS lead to oxidative damage in biomolecules (especially in proteins, lipids, and DNA). These injuries cause various clinical disorders such as cardiovascular disease, aging and neurological damage such as Alzheimer's, Parkinson's, genetic mutations and cancer [25–28]. Living organisms have developed a complex antioxidant network to neutralize reactive oxygen species that are harmful to human life. Several enzyme-dependent systems can detoxify free radicals; For example, superoxide dismutase containing copper and zinc catalyzes the conversion of

Table 1
The IC$_{50}$ of Fe$_3$O$_4$@PJ/Ag NPs and BHT in the antioxidant test.

	Fe$_3$O$_4$@PJ/Ag NPs	BHT
IC$_{50}$ (μg/mL)	122 ± 0[a]	101 ± 0[a]
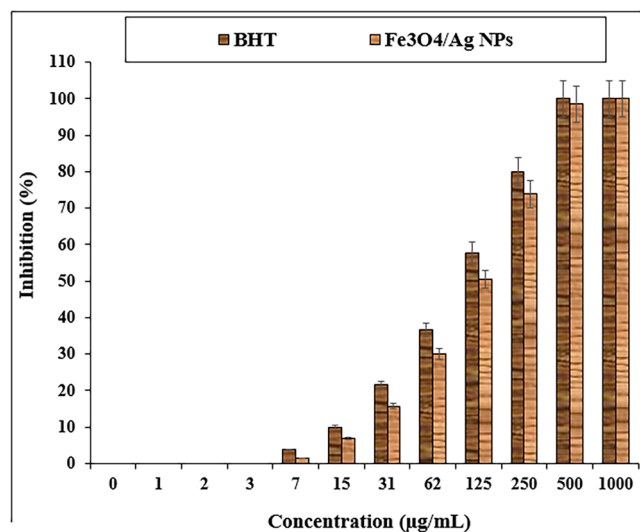
Fig. 7. The antioxidant properties of Fe$_3$O$_4$@PJ/Ag NPs and BHT against DPPH.

superoxide anion into hydrogen peroxide, and then enzymes such as catalase and glutathione peroxidase remove hydrogen peroxide from the environment by converting it to water and oxygen [29–31]. In addition, some antioxidant compounds in food can be a barrier against free radical damage by preventing the formation of radicals, absorbing free radicals or accelerating their destruction [30–33]. Antioxidants are compounds that effectively and in different ways prevent the reaction of free radicals in the form of active oxygen and nitrogen with biomolecules such as protein, amino acid, lipid and DNA and lead to the reduction of damage or cell death, cardiovascular diseases and cancers. In addition to their role in biological systems, in foods rich in unsaturated fats, they also prevent the reduction of nutritional quality, safety, bad taste and discoloration due to the creation of toxic compounds. Antioxidants are divided into two categories: chemical and natural [32–36]. The most widely used chemical antioxidants in the food industry include TBHQ, BHA, BHT, and propyl gallate, which are known to cause cancer and have negative effects on human health. Therefore, nowadays, the use of a wide group of biological nanoparticles as therapeutic sources that have antioxidant properties has attracted the attention of researchers [14–17].

The DPPH radical scavenging aptitude of Fe$_3$O$_4$@PJ/Ag NPs and BHT has been expressed in terms of % inhibition, being represented in Table 1 and Fig. 7. Evidently, the capacity gradually increases with increasing the sample concentration and becomes the maximum at 1000 μg/mL (99.8 %). The oxygenated and nitrogenous organic functional groups in the phytomolecules and also the electron source over the Ag and Fe$_3$O$_4$ NPs facilitate the quenching of DPPH bare radicals thus fading out of its original color (purple to pale yellow). The capacity is absolutely comparable to the molecular standard BHT. Table 1 also displays the corresponding inhibitory concentration at half maxima as 122, whereas the standard shows a value of 101.

In the cytotoxicity and anti-cancer investigation, the corresponding GC1415, NCI-N87 and MKN45 gastric cancer cell lines were treated with Fe$_3$O$_4$@PJ/Ag NPs at different concentrations, being assessed by MTT studies for 48 h. The ineffectiveness of the material on the normal cell line was also validated over normal HUVEC cell lines. The % cell
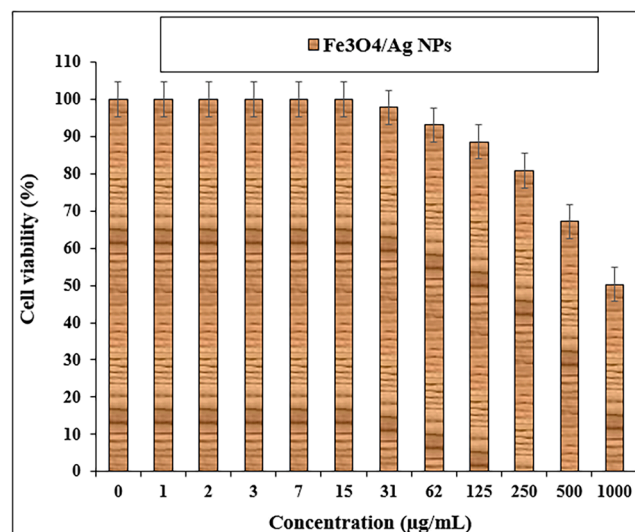
Fig. 8. The cytotoxicity properties of Fe$_3$O$_4$@PJ/Ag NPs against HUVEC cell line.
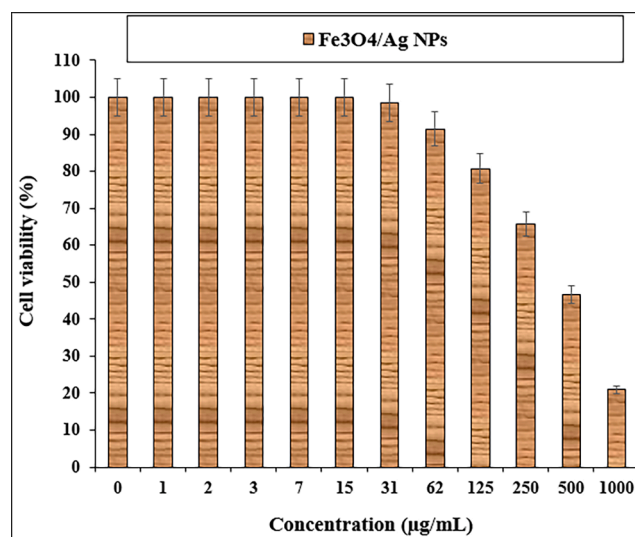
Fig. 9. The anti-human gastric cancer properties of Fe$_3$O$_4$@PJ/Ag NPs against GC1415 cell line.

viability was determined by measuring the absorbances spectrophotometrically at a wavelength 570 nm. The results have been displayed in Fig. 8-11 and Table 2.

The % cell viability of malignant gastric cell line reduced dose-dependently in the presence of Fe$_3$O$_4$@PJ/Ag NPs. The IC$_{50}$ of Fe$_3$O$_4$@PJ/Ag NPs were 456, 482, and 345 μg/mL against GC1415, NCI-N87 and MKN45 cell lines, respectively (Table 2 and Figs. 9-11).

As indicated in Fig. 12, our results showed that Fe$_3$O$_4$@PJ/Ag NPs induce a remarkable cell cycle arrest at the S phase, with a significant reduce in G2/M and G0/G1 cancer cell lines phases, revealing cell-cycle progression inhibition under the effect of Fe$_3$O$_4$@PJ/Ag NPs.

Our cell apoptosis results indicate that Fe$_3$O$_4$@PJ/Ag NPs remarkably induces late and early apoptosis in a dose-dependent manner in gastric cancer cell lines (Fig. 13).

As shown in Fig. 14, our colony formation results indicate a remarkable reduce in the colonies number for gastric cancer cell lines under the colony formation effect compared to the control. These data confirm colony-forming ability loss in gastric cancer cell lines upon treatment with Fe$_3$O$_4$@PJ/Ag NPs, which may affect the ability to
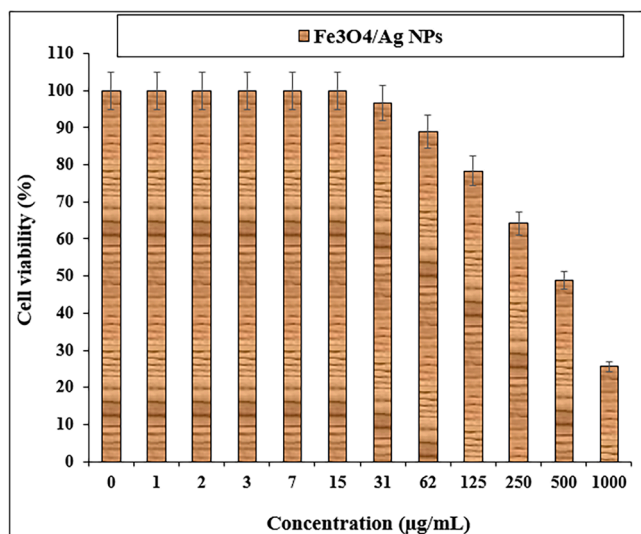
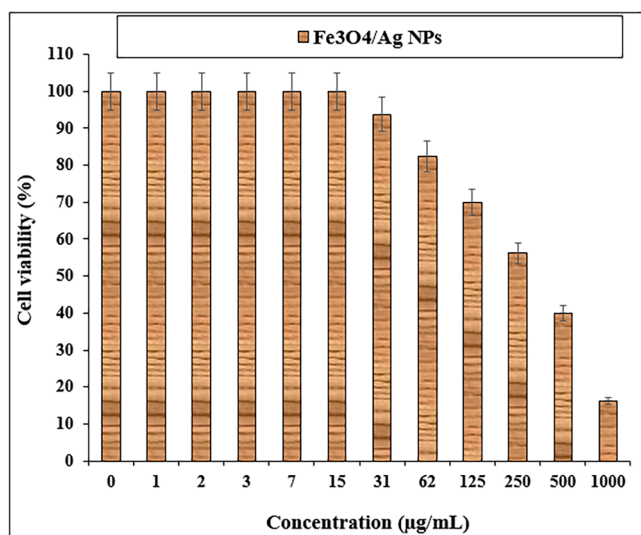**Fig. 10.** The anti-human gastric cancer properties of Fe_3O_4@PJ/Ag NPs against NCI-N87 cell line.

Fig. 11. The anti-human gastric cancer properties of Fe_3O_4@PJ/Ag NPs against MKN45 cell line.

Table 2
The IC50 of Fe_3O_4@PJ/Ag NPs in the anti-human gastric cancer test.

	HUVEC	GC1415	NCI-N87	MKN45
IC50 (µg/mL)	–	456 ± 0^b	482 ± 0^b	345 ± 0^a

prevent tumorigenesis *in vivo*.

Western blot analysis data indicated a remarkableraise inthe pro-apoptotic markers expression (Cleavedcaspase-8andBax) in Fe_3O_4@PJ/Ag NPs-treated cells compared to control (Fig. 15). Also, the anti-apoptoticprotein expression (Bcl-2) was decreased in gastric cancer cell lines. Bax/Bcl-2 ratio was raised profoundly in cells treated with Fe_3O_4@PJ/Ag NPs.

Also, we assessed the p53, STAT3 andp-STAT-3 expression pattern in gastric cancer cell lines exposed to Fe_3O_4@PJ/Ag NPs. We observed that the treatment with this magnetite nanoparticles stimulates the p53 expression pattern whereas, it inhibits the STAT3 phosphorylation and expression in gastric cancer cell lines as compared with control cells.
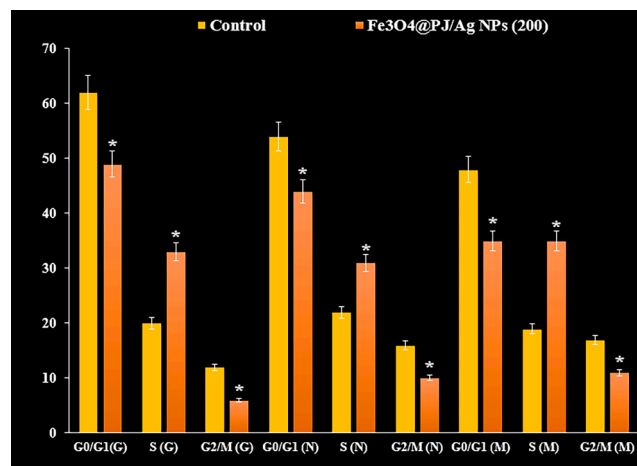

Fig. 12. Cell cycle flow cytometry analysis (%) of the gastric cancer cell lines. (G): GC1415, (N): NCI-N87, (M): MKN45.
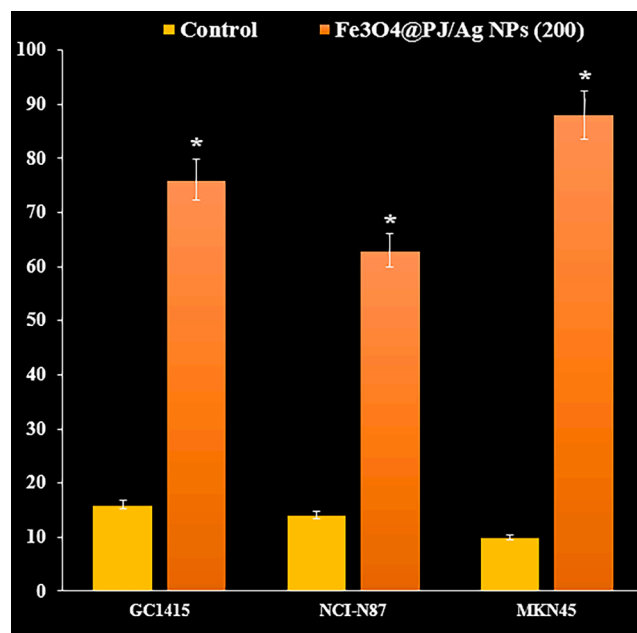

Fig. 13. Induction of apoptosis (%).

The exact molecular mechanisms of anticancer effects of nanoparticles are not yet fully understood. Therefore, researchers are working to treat cancer and to activate the mechanism of planned death [28–31]. Induction of apoptosis in cancer cells is one of the functional mechanisms of drugs used in chemotherapy and is essential in the treatment of cancer. Nanoparticles increase the amount of intracellular free radicals, so oxidative stress can be considered as a response to cell damage [28–31]. The production of free radicals for each nanoparticle has a different cellular and molecular mechanism. Oxidative stress can activate or inhibit a number of antioxidant enzymes in the cell. The activity of superoxide dismutase and catalase enzymes, which are part of the antioxidant defense system and play a very important role in suppressing reactive oxygen species, continues that they were studied as biomarkers of oxidative stress [27–34].

4. Conclusion

In summary, we demonstrate a green and biogenic procedure for the in *situ* immobilization of Ag NPs over the Fe_3O_4 NPs mediated by
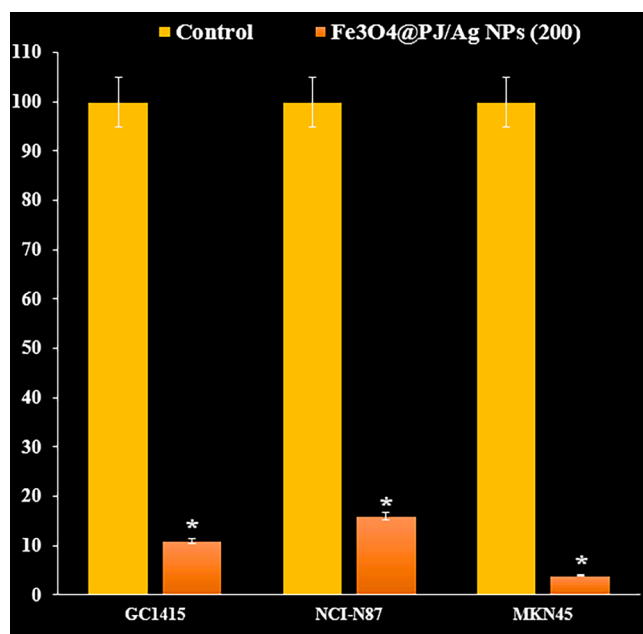
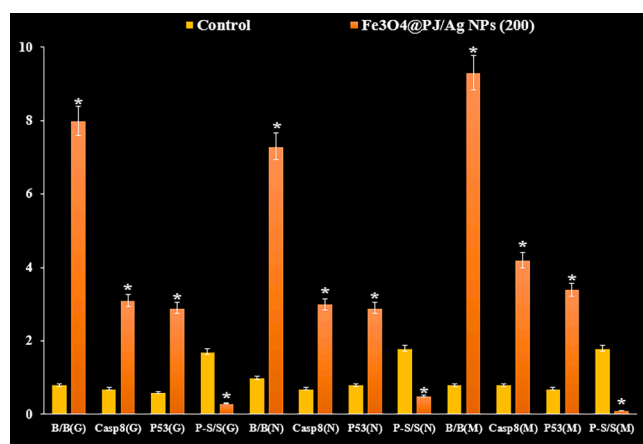**Fig. 14.** The effect of Fe$_3$O$_4$@PJ/Ag NPs (200) on colony formation (%).

Fig. 15. Outcome of Fe$_3$O$_4$@PJ/Ag NPs (200) on the expression patterns of Bax, BCL-2, Caspase-8, P53 and STAT3. (G): GC1415, (N): NCI-N87, (M): MKN45, P—S/S: P-STAT3/STAT3, B/B: Bax/Bcl2.

Pomegranate juice, without the involvement of any unsafe and hazardous chemicals following a post-functionalization approach (Fe$_3$O$_4$@PJ/Ag NPs). The physicochemical features of the material were analyzed over a range of analytical techniques. It was explored biologically in the study of anti-cancer effects over gastric cancer cell lines GC1415, NCI-N87 and MKN45 and also the normal HUVEC cell line. The % cell viability of malignant cancer cell lines reduced dose-dependently in the presence of Fe$_3$O$_4$@PJ/Ag NPs. Again, in the antioxidant studies the Fe$_3$O$_4$@PJ/Ag NPs showed excellent potential against DPPH free radical. So, the findings of the recent research show that biologically synthesized Fe$_3$O$_4$@PJ/Ag NPs might be used to cure gastric cancer. In addition, the current study offer that Fe$_3$O$_4$@PJ/Ag NP scould be a new potential adjuvant chemopreventive and chemotherapeutic agent against cytotoxic cells.

Data Availability Statement.

Data available on request from the authors.

Declaration of Competing Interest

The authors declare that they have no known competing financial interests or personal relationships that could have appeared to influence the work reported in this paper.

Data availability

Data will be made available on request.

References

[1] I. Hilger, W.A. Kaiser, Iron oxide-based nanostructures for MRI and magnetic hyperthermia, Nanomedicine. 7 (2012) 1443–1459.

[2] V. Orel, A. Shevchenko, A. Romanov, M. Tselepi, T. Mitrelias, C.H. Barnes, A. Burlaka, S. Lukin, I. Shchepotin, Magnetic properties and antitumor effect of anocomplexes of iron oxide and doxorubicin, Nanomedicine. 11 (2015) 47–55.

[3] F.K. Van Landeghem, K. Maier-Hauff, A. Jordan, K.-T. Hoffmann, U. Gneveckow, R. Scholz, B. Thiesen, W. Brück, A. von Deimling, Post-mortem studies in glioblastoma patients treated with thermotherapy using magnetic nanoparticles, Biomaterials 30 (2009) 52–57.

[4] Silva A.C., Oliveira T.R., Mamani J.B., Malheiros S.M., Malavolta L., Pavon L.F., Sibov T.T., Amaro E., Jr., Tann_us A., Vidoto E.L. Application of hyperthermia induced by superparamagnetic iron oxide nanoparticles in glioma treatment. Int. J. Nanomed. 2011;6:591–603.

[5] (a) Y. Yildiz, T. Onal Okyay, B. Sen, B. Gezer, S. Kuzu, A. Savk, E. Demir, Z. Dasdelen, H. Sert, F., Sen ChemistrySelect 2 (2017) 697–701;
(b) F. Göl, A. Aygün, A. Seyrankaya, T. Gür, C. Yenikaya, F. Şen, Mater. Chem. Phys. 250 (2020) 123037;
(c) F. Gulbagca, S. Ozdemir, M. Gulcan, F. Sen, Heliyon 5 (12) (2019) e02980;
(d) A. Aygün, F. Gülbağca, M.S. Nas, M.H. Alma, M.H. Çalımlı, B. Ustaoglu, Y. C. Altunoglu, M.C. Baloğlu, K. Cellat, F. Şen, J. Pharm. Biomed. Anal. 179 (2020) 113012;
(e) A. Aygün, F. Gülbağça, L.Y. Ozer, B. Ustaoglu, Y.C. Altunoglu, M.C. Baloğlu, M. N. Atalar, M.H. Alma, F. Sen, J. Pharm. Biomed. Anal. 179 (2020) 112961;
(f)N. Korkmaz, Y. CeylanY. Ceylan, A. Hamid, A. Karadağ, A. S. Bülbül, M. N. Aftab, Ö. Çevik, F. Şen, Journal of Drug Delivery Science and Technology 2020, 59, 101864.(g) B. Sen, A. Şavk, F. Sen, J. Colloid Interface Sci. 520 (2018) 112–118;
(h) B. Şen, A. Aygün, A. Şavk, S. Akocak, F. Şen, Int. J. Hydrogen Energy 43 (44) (2018) 20183–20191;
(i) B. Sen, E. Kuyuldar, B. Demirkan, T.O. Okyay, A. Şavk, F. Sen, J. Colloid Interface Sci. 526 (2018) 480–486.

[6] a) S. Mirfakhraei, M. Hekmati, F.H. Eshbala, H. Veisi, New Journal of Chemistry 42, 2018, 1757-1761; b) H. Veisi, S. Kazemi, P. Mohammadi, P. Safarimehr, S. Hemmati, Polyhedron 157, 2019, 232-240;c) B. Maleki, S. Hemmati, A. Sedrpoushan, S.S. Ashrafi, H. Veisi. RSC Adv. 2014, 4 (76), 40505-40510;d)M. Hamelian, S. Hemmati, K. Varmira, H. Veisi, Journal of the Taiwan Institute of Chemical Engineers 2018, 93, 21-30; e) H. Veisi, S. Hemmati, H. Shirvani, H. Veisi, Applied Organometallic Chemistry 2016, 30, 387-391; f)H. Veisi, Current Organic Chemistry 15 (2011) 2438-2468; g)H. Veisi, B. Karmakar, T. Tamoradi, S. Hemmati, M. Hamelian, Scientific Reports 11 (2021) 1-13; h)M. Baghayeri, R. Ansari, M. Nodehi, H. Veisi, International Journal of Environmental Analytical Chemistry 98 (2018), 874-888.

[7] S. Klein, A. Sommer, L.V. Distel, J.L. Hazemann, W. Kröner, W. Neuhuber, P. Müller, O. Proux, C. Kryschi, Superparamagnetic iron oxide nanoparticles as novel X-ray enhancer for low-dose radiation therapy, J. Phys. Chem. B. 118 (2014) 6159–6166.

[8] D.K. Chatterjee, L.S. Fong, Y. Zhang, Nanoparticles in photodynamic therapy: An emerging paradigm, Adv. Drug Deliv. Rev. 60 (2008) 1627–1637.

[9] A.P. Zhang, Y.P. Sun, Photocatalytic killing effect of TiO$_2$ nanoparticles on Ls- 174-t human colon carcinoma cells, World J. Gastroenterol. 10 (2004) 3191–3193.

[10] P. Thevenot, J. Cho, D. Wavhal, R.B. Timmons, L. Tang, Surface chemistry influences cancer killing effect of TiO$_2$ nanoparticles, Nanomedicine. 4 (2008) 226–236.

[11] J. Colon, N. Hsieh, A. Ferguson, P. Kupelian, S. Seal, D.W. Jenkins, C.H. Baker, Cerium oxide nanoparticles protect gastrointestinal epithelium from radiation-induced damage by reduction of reactive oxygen species and upregulation of superoxide dismutase 2, Nanomedicine. 6 (2010) 698–705.

[12] M.S. Wason, J. Colon, S. Das, S. Seal, J. Turkson, J. Zhao, C.H. Baker, Sensitization of pancreatic cancer cells to radiation by cerium oxide nanoparticle-induced ROS production, Nanomedicine. 9 (2013) 558–569.

[13] R.W. Tarnuzzer, J. Colon, S. Patil, S. Seal, Vacancy engineered ceria nanostructures for protection from radiation-induced cellular damage, Nano Lett. 5 (2005) 2573–2577.

[14] D. Ali, S. Alarifi, S. Alkahtani, A.A. AlKahtane, A. Almalik, Cerium oxide nanoparticles induce oxidative stress and genotoxicity in human skin melanoma cells, Cell Biochem. Biophys. 71 (2014) 1643–1651.

[15] D. Neri, C.T. Supuran, Interfering with pH regulation in tumors as a therapeutic strategy, Nat. Rev. Drug Discov. 10 (2011) 767–777.

[16] J.W. Seo, H. Chung, M.Y. Kim, J. Lee, I.H. Choi, J. Cheon, Development of watersoluble single-crystalline TiO$_2$ nanoparticles for photocatalytic cancer-cell treatment, Small. 3 (2007) 850–853.

[17] Z. Hou, Y. Zhang, K. Deng, Y. Chen, X. Li, X. Deng, Z. Cheng, H. Lian, C. Li, J. Lin, UV-emitting upconversion-based TiO2 photosensitizing nanoplatform: Near-infrared light mediated *in vivo* photodynamic therapy via mitochondria-involved apoptosis pathway, ACS Nano 9 (2015) 2584–2599.

[18] S. Cui, D. Yin, Y. Chen, Y. Di, H. Chen, Y. Ma, S. Achilefu, Y. Gu, *In vivo* targeted deep-tissue photodynamic therapy based on near-infrared light triggered upconversion nanoconstruct, ACS Nano 7 (2013) 676–688.

[19] S.S. Lucky, N.M. Idris, Z. Li, K. Huang, K.C. Soo, Y. Zhang, Titania coated upconversion nanoparticles for near-infrared light triggered photodynamic therapy, ACS Nano 9 (2015) 191–205.

[20] (a) S. Özliman, S. Moradi, M. Pirhadi, B.S. Rabeea, Plant Biotechnol Persa. 3 (2) (2021) 63–67;
(b) S. Rabeea Banoon, M. Narimani-Rad, A. Lotfi, S. Shokri, S. Abbaszadeh, S. Özliman, Plant Biotechnol Persa. 3 (2) (2021) 68–74;
(c) H. Ghaneialvar, N. Abbasi, S. Saneei, A. Zangeneh, M.M. Zangeneh, M. Pooyanmehr, et al., Plant Biotechnol Persa. 3 (1) (2021) 1–8;
(d) N. Abbasi, H. ghaneialvar, S. Saneei, M.M. zangeneh, A. zangeneh, Plant Biotechnol Persa. 3 (1) (2021) 9–17;
(e) S. Vivekanandarajah, P. Rajamanoharan, Plant Biotechnol Persa. 3 (1) (2021) 18–25;
(f) A. Sardashti, A. Sardashti, Plant Biotechnol Persa. 3 (1) (2021) 26–33;
(g) M. Karimi, M. Gholami-Ahangaran, Plant Biotechnol Persa. 3 (1) (2021) 34–36;
(h) S. Shahsavari, Plant Biotechnol Persa. 3 (1) (2021) 37–38;
(i) F. Magbool, E.M.E.S. Ibrahim Elnima, I.E. Hamedelniel, A. Mahmoud, A. Gamil, E.M. Adam, et al., Plant Biotechnol Persa. 2 (2) (2020) 1–13;
(j) N. Farhad, S. Shahsavari, Plant Biotechnol Persa. 2 (2) (2020) 21–23.

[21] Stewart B., Wild C.P. World Cancer Report 2014. International Agency for Research on Cancer World Health Organization; Lyon, France: 2014. [(accessed on 24 March 2015)]. Available online: http://www.iarc.fr/en/publications/books/wcr/wcr-order.php.

[22] J.W. Rasmussen, E. Martinez, P. Louka, D.G. Wingett, Zinc oxide nanoparticles for selective destruction of tumor cells and potential for drug delivery applications, Exp. Opin. Drug Deliv. 7 (2010) 1063–1077.

[23] B. Felice, M.P. Prabhakaran, A.P. Rodríguez, S. Ramakrishna, Drug delivery vehicles on a nano-engineering perspective, Mater. Sci. Eng. C. 41 (2014) 178–195.

[24] E. Fernandes, J.A. Ferreira, A. Peixoto, L. Lima, S. Barroso, B. Sarmento, L. L. Santos, New trends in guided nanotherapies for digestive cancers: A systemic review, J. Control Release. 209 (2015) 288–307.

[25] F. Caputo, M. de Nicola, L. Ghibelli, Pharmacological potential of bioactive engineered nanomaterials, Biochem. Pharmacol. 92 (2014) 112–130.

[26] F. Danhier, O. Feron, V. Preat, To exploit the tumor microenvironment: Passive and active tumor targeting of nanocarriers for anti-cancer drug delivery, J. Control Release. 148 (2010) 135–146.

[27] (a) M.M. Zangeneh, Appl. Organometal. Chem. 33 (2019) e5295, https://doi.org/10.1002/aoc.5295;
(b) G. Mohammadi, M.M. Zangeneh, A. Zangeneh, Z.M. Siavosh Haghighi, Appl. Organometal Chem. 33 (2019) e5136, https://doi.org/10.1002/aoc.5136;
(c) M.M. Zangeneh, S. Bovandi, S. Gharehyakheh, A. Zangeneh, P. Irani, Appl. Organometal. Chem. 33 (2019) e4961;
(d) M.M. Zangeneh, Z. Joshani, A. Zangeneh, E. Miri, Appl. Organometal. Chem. 33 (2019) e5016;
(e) A. Zangeneh, M.M. Zangeneh, R. Moradi, Appl. Organometal. Chem. 33 (2019) e5247, https://doi.org/10.1002/aoc.5247.

[28] (a) M.M. Zangeneh, A. Zangeneh, E. Pirabbasi, R. Moradi, M. Almasi, Appl. Organometal. Chem. 33 (2019) e5246, https://doi.org/10.1002/aoc.5246;
(b) B. Mahdavi, S. Paydarfard, M.M. Zangeneh, S. Goorani, N. Seydi, A. Zangeneh, Appl. Organometal. Chem. 33 (2019) e5248, https://doi.org/10.1002/aoc.5248;
(c) A.R. Jalalvand, M. Zhaleh, S. Goorani, M.M. Zangeneh, N. Seydi, A. Zangeneh, R. Moradi, J. Photochem. Photobiol. B. 192 (2019) 103–112;
(d) A. Zangeneh, M.M. Zangeneh, Appl. Organometal. Chem. 33 (2019) e5290, https://doi.org/10.1002/aoc.5290.

[29] J. Kolosnjaj-Tabi, R. di Corato, L. Lartigue, I. Marango, P. Guardia, A.K. Silva, N. Luciani, O. Clément, P. Flaud, J.V. Singh, et al., Heat-generating iron oxide nanocubes: Subtle "destructurators" of the tumoral microenvironment, ACS Nano 8 (2014) 4268–4283.

[30] S. Bhattacharyya, R.A. Kudgus, R. Bhattacharya, P. Mukherjee, Inorganic nanoparticles in cancer therapy, Pharm Res. 28 (2011) 237–259.

[31] J. Chen, S. Patil, S. Seal, J.F. McGinnis, Rare earth nanoparticles prevent retinal degeneration induced by intracellular peroxides, Nat. Nanotechnol. 1 (2006) 142–150.

[32] M. Das, S. Patil, N. Bhargava, J.F. Kang, L.M. Riedel, S. Seal, J.J. Hickman, Auto-catalytic ceria nanoparticles offer neuroprotection to adult rat spinal cord neurons, Biomaterials 28 (2007) 1918–1925.

[33] C. Korsvik, S. Patil, S. Seal, W.T. Self, Superoxide dismutase mimetic properties exhibited by vacancy engineered ceria nanoparticles, Chem. Commun. 1056–1058 (2007).

[34] R. Hong, G. Han, J.M. Fernandez, B.J. Kim, N.S. Forbes, V.M. Rotello, Glutathione-mediated delivery and release using monolayer protected nanoparticle carriers, J. Am. Chem. Soc. 128 (2006) 1078–1079.

[35] A.R. Jalalvand, M. Zhaleh, S. Goorani, M.M. Zangeneh, N. Seydi, A. Zangeneh, R. Moradi, J. Photochem. Photobiol. B.: Biol. 192 (2019) 103–112.

[36] (a) M.M. Zangeneh, A. Zangeneh, E. Pirabbasi, R. Moradi, M. Almasi, Appl. Organometal. Chem. 33 (2019) e5246;
(b) H. Kheraldine, I. Gupta, H. Alhussain, A. Jabeen, F.S. Cyprian, S. Akhtar, et al., Substantial cell apoptosis provoked by naked PAMAM dendrimers in HER2-positive human breast cancer via JNK and ERK1/ERK2 signalling pathways, Comput. Struct. Biotechnol. J. 19 (2021) 2881–2890.